Methane Conversion Rate into Structure H Hydrate Crystals from Ice

Robin Susilo
Steacie Institute for Molecular Sciences, National Research Council Canada, Ottawa, ON, Canada K1A 0R6
Dept. of Chemical and Biological Engineering, University of British Columbia, Vancouver, BC, Canada V6T 1Z3

John A. Ripmeester
Steacie Institute for Molecular Sciences, National Research Council Canada, Ottawa, ON, Canada K1A 0R6

Peter Englezos
Dept. of Chemical and Biological Engineering, University of British Columbia, Vancouver, BC, Canada V6T 1Z3

DOI 10.1002/aic.11268
Published online July 27, 2007 in Wiley InterScience (www.interscience.wiley.com).

The methane uptake and conversion rate to structure H (sH) hydrates was measured and compared to crystallization kinetics models. Three large molecule guest substances (LMGS) were used as sH hydrate formers: neohexane (NH), methylcyclohexane (MCH), and tert*-butyl methyl ether* (TBME). *The initial crystallization occurred quickly at the LMGS liquid-ice interface until ~20–30% of ice was converted into hydrate (hydrate growth stage I). Slower hydrate crystal growth was observed after a hydrate film covered the ice surface at a rate of 3–400 nm^2/h (hydrate growth stage II). The TBME system showed the fastest kinetics at the beginning of the reaction followed by NH and MCH system. However the trend changed when the temperature was increased ("reaction" stage III). Surprisingly, the conversion rate achieved with the TBME system upon melting the ice was the smallest. This was attributed to the strong interaction of TBME with water molecules that increased the energy barrier for water molecules to form hydrate cages. The conversion rates were well correlated with the Avrami equation and the shrinking core model. Finally, NH was found to be the best LMGS in this study to obtain full conversion within a short reaction time and achieving high methane gas storage in the hydrate.* © 2007 American Institute of Chemical Engineers *AIChE J,* 53: 2451–2460, 2007
Keywords: structure H hydrate, hydrate kinetics, hydrate conversion, methane, gas storage

Introduction

Storing and transporting natural gas via gas hydrates is one of the applications based on hydrate technology that continues to receive attention.[1–3] The economical evaluation of such a hydrate-based technology are also promising.[4–6] However more investigation is still required to establish the technology. In particular, finding the operating conditions which may offer the fastest hydrate kinetics/conversion rates and high gas storage capacity with high hydrate stability are important. Methane is the main component of natural gas and is considered as a clean energy source. It is a simple molecule that is small enough to fit all cavities in the hydrate lattices. Methane with water generally forms cubic structure I (sI)

Correspondence concerning this article should be addressed to P. Englezos at englezos@interchange.ubc.ca.

hydrate under moderate pressure and low temperature conditions,[7] although cubic structure II (sII) methane hydrate was also reported as a meta-stable material.[8] Methane in hexagonal structure H (sH) hydrate may also exist at extremely high pressure[9] with two to five methane molecules the suggested large cage occupancy.[10,11] The presence of other molecules may also alter the hydrate structure and methane occupancy of the hydrate phase. Kinetics and thermodynamics both govern how methane molecules occupy the hydrate cages and stabilize the crystal structure. Because this determines the methane content and the ultimate storage capacity of hydrates, a careful consideration of the hydrate formation conditions and systems are needed for a particular industrial application.

Recently, significant research efforts have been devoted to study the possibility of storing methane as sH hydrate. This is due to the fact that sH hydrate has a lower hydrate formation pressure than sI and high gas storage potential.[12] However, only few studies have addressed the kinetics out of the many publications on phase equilibria. Moreover, hydrate conversion from the feed water/ice used in the experiment is seldom reported. Our earlier work through gas uptake measurements[13] and NMR spectroscopy[14] revealed that the kinetics depends on the chosen large molecule guest substance (LMGS) and the driving force, which is essentially the deviation of the formation pressure from the equilibrium pressure at a given temperature. Unfortunately, in both studies the hydrate conversions obtained were still far from completion. Water occlusion is typically encountered once hydrate starts forming and that significantly impedes the subsequent crystal growth. Forming hydrate from ice may offer higher hydrate conversion especially with thermal ramping across the icepoint. Through the NMR study, it was found that the wetting of LMGS and ice packing density influence the hydrate conversion rate.

Hence the objective of this study is to follow up on the previous NMR work, which is to form hydrate in bulk samples and find out if full hydrate conversion can be achieved in a reasonable timeframe. Fresh-ground ice powder with loose ice packing density was used to synthesize hydrates. Methane uptake during hydrate formation was measured and the conversion rates were correlated to crystallization kinetics models. Two different hydrate formation pressures and the LMGS amounts were chosen to see how they may influence the kinetics. In addition, a mixture of LMGSs was also studied to investigate if the kinetics can be improved while maintaining the gas content in the hydrate phase.

Experimental Apparati and Procedures

Hydrates were synthesized from fresh-ground ice particles ($\sim$1.3 μm) that were poured by gravity into a 50 ml pressure vessel. Approximately 10 g of ice powder was used with the LMGS sprayed by a syringe from the top after loading the ice powder. The expected total moles of methane uptake if ice was fully converted to hydrate are $\sim$82 mmol for sH hydrate and $\sim$97 mmol for sI hydrate when all cages are fully occupied. The gas amount is less and has to be adjusted accordingly when the methane occupancies in the hydrate cages are not full. It was noted that ice particles almost filled the vessel completely. The LMGS amount was varied to be 200% (excess) and 50% as calculated for the stoichiometric amount. Additional experiments were also conducted by adding TBME as a polar guest to a hydrophobic guest (NH) with relative concentrations of 1:6 and 1:3. The list of chemicals/LMGSs used in this study is summarized in Table 1. The loading procedure was performed in a freezer at $\sim$253 K to prevent melting of the ice. The vessel was then immersed in a constant temperature water bath and connected to a valve and pressure transducer. The time zero of the measurement was recorded as the vessel was pressurized to the desired pressure. All measurements were performed at 253 K for about 20 h. At the end of the 20-h period the temperature was increased to a point above the icepoint (274 K) within 5 min to enhance the conversion of ice into hydrate. It is well known that temperature ramping enhances the conversion to hydrate.[15] Two starting pressure conditions (P_0) were chosen, $\sim$4.3 (low pressure condition) and 8.1 MPa (high pressure condition) which would give final pressures at the end of the experiment well below and above the equilibrium condition for sI methane hydrate at 274 K (P_{eq} = $\sim$2.9 MPa). The starting pressures were well above the stability region of sI hydrate to ensure there was sufficient methane to convert ice into hydrate. This is because the experiment was conducted in a pressure vessel without replenishment of the gas supply, so the pressure kept dropping as the hydrate formed. The experiments were stopped when a significant pressure drop was no longer observed (almost full hydrate conversion was achieved). The moles of methane uptake over time were calculated from the pressure drop profile in the vessel with respect to the starting pressure, taking the gas compressibility into account. The equations used are given elsewhere.[13]

Results and Discussion

A typical pressure drop profile recorded during hydrate formation is shown in Figure 1. The pressure dropped relatively fast in the first few hours indicating rapid hydrate formation. Ice surfaces were in contact directly with the LMGS liquid so that methane diffusion in LMGS and intrinsic kinetics controlled the initial reaction (reaction stage I). A noticeable induction time was not observed for any of the systems investigated. The pressure drop slowed considerably presumably because a hydrate film covered the ice surface. Thus the reaction became limited by the diffusion of methane and LMGS across the hydrate film and the reaction at the ice-hydrate interface (reaction stage II). The ramping of temperature above the icepoint increased the pressure before dropping back down again. The thermal ramping enhanced the transformation of the unreacted ice core towards complete transformation (reaction stage III) into hydrate. The

Table 1. List of Chemicals Used in This Work

Chemical	Certified Purity	Supplier
Methane	UHP grade	Praxair
tert-butyl methyl ether (TBME)	99.9%	Sigma Aldrich
Neohexane (NH)	99%+	Sigma Aldrich
Methylcyclohexane (MCH)	99%+	Sigma Aldrich
n-heptane (nC_7)	99%+	Omnisolv
Water	Distilled	

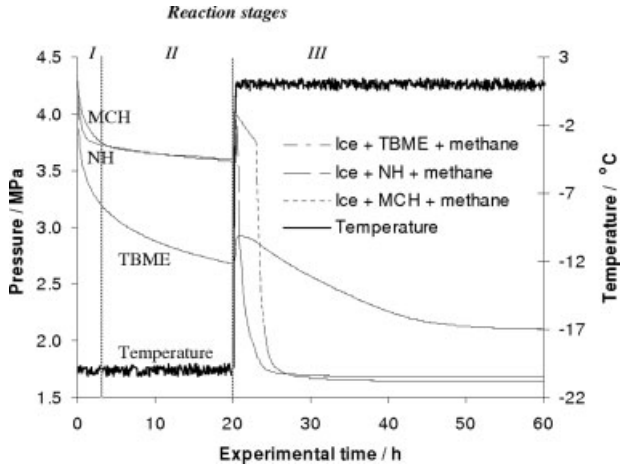

Figure 1. Pressure drop profile during hydrate formation from ice + LMGS (~200%) + methane synthesized at low pressure (P_0 = ~4.3 MPa).

The LMGS used are *tert*-butyl methyl ether (TBME), neohexane (NH), and methylcyclohexane (MCH).

pressure drop data was then used to calculate the moles of methane gas in the hydrate phase, as shown in Figure 2. Rapid methane gas uptake is seen in reaction stage I and then followed by a slower rate in stage II because of mass transfer resistance. The melting of un-reacted ice inside the hydrate shell allows new contact sites that allow further reaction towards completion (stage III).

The conversion rate of ice/water into hydrate can also be calculated if the hydrate structure formed and cage occupancy values for methane and LMGS in the hydrate phase are known. Hence it is important to have such information. A detailed solid phase analysis of hydrates synthesized in this study is reported elsewhere.[16] Table 2 shows a summary of the cage occupancy values and Table 3 the gas content in

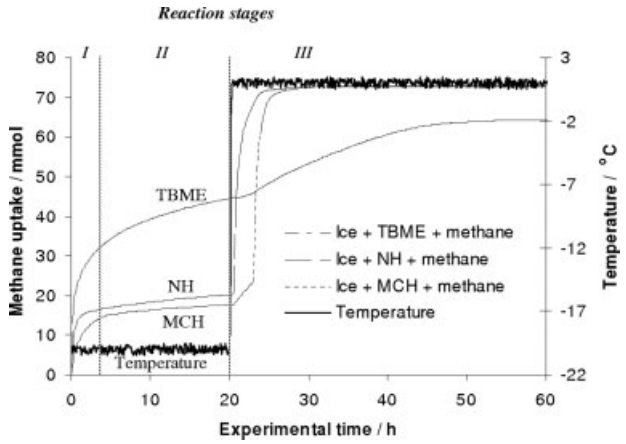

Figure 2. Amount of methane uptake during hydrate formation from ice + LMGS (~200%) + methane synthesized low pressure (P_0 = ~4.3 MPa).

The LMGS used are *tert*-butyl methyl ether (TBME), neohexane (NH), and methylcyclohexane (MCH).

Table 2. Summary of Cage Occupancy Values Obtained by ^{13}C Solid State NMR[16]

LMGS Used	Final Pressure, MPa at 274 K	Hydrate Structure	θ_S, %	θ_M, %	θ_L, %
No LMGS	~6	I	87	–	100
TBME (200%)	~2	H	78	76	100
	~6	H	97	79	100
NH (200%)	~2	H	88	88*	100
	~6	H	99	99*	100
MCH (200%)	~2	H	90	90*	100
	~6	H	100	100*	100
3NH:1TBME (200%)	~2	H	76	76*	100
6NH:1TBME (200%)	~2	H	88	88*	100

*The spectra from NMR do not distinguish the methane in the small and medium cages because of very close chemical shift and broader peak than TBME system. Hence the average occupancy from the two cages is reported.

the hydrate phase.[16] The solid-state analysis at the end of the experiment revealed the presence of methane in sH hydrate for all systems. A mixture of sI and sH hydrate was observed only in the system with LMGS amounts less than stoichiometric. Figure 3 shows the conversion versus time calculated from the gas uptake showed in Figure 2. The conversion is calculated based on the mol uptake data divided by the total mol of methane that would be enclathrated if all ice/water that is present in the system is fully converted into hydrate. It is important to note here that the hydrate structure and cage occupancies were assumed to remain the same throughout the experiments. This assumption is reasonable when the system has excess of LMGS because the expected hydrates formed are sH only. However the calculated conversion values may be under or over estimated for the mixed sI and sH hydrates. It is not known how and when the mixed hydrate is formed, whether simultaneously or subsequently after the shortage of LMGS.

Methane uptake with 200% LMGS amount synthesized at low pressure (P_0 = ~4.3 MPa)

Examination of the results in Figures 2 and 3 reveals two types of hydrate growth behavior. The systems with NH and MCH have similar hydrate growth trends most likely because they are both hydrophobic molecules. The observed kinetics was relatively slow at 253 K but then rapid hydrate growth

Table 3. Gas Content in Hydrate Phase Measured by Decomposition Under Vacuum Condition[16]

LMGS Used	Pressure	Gas/Hydrate (v/v)	Gas/Water (v/v)
No LMGS	High	173	210
TBME (200%)	Low	103	131
	High	125	160
NH (200%)	Low	130	166
	High	139	177
MCH (200%)	Low	132	168
	High	142	181
3NH:1TBME (200%)	Low	109	139
6NH:1TBME (200%)	Low	123	157

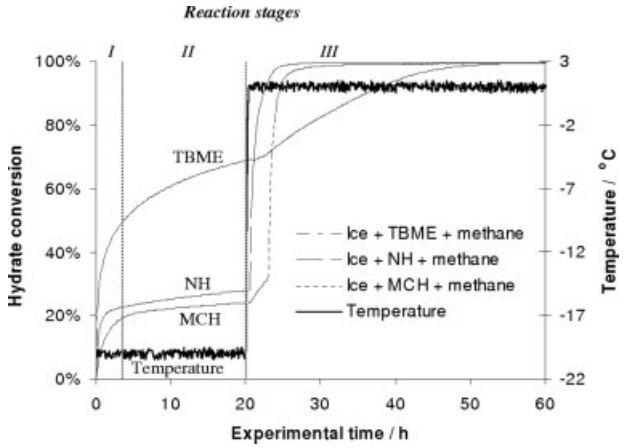

Figure 3. Hydrate conversion rate of ice + LMGS (~200%) + methane synthesized at low pressure (P_0 = ~4.3 MPa).

The LMGS used are *tert*-butyl methyl ether (TBME), neohexane (NH), and methylcyclohexane (MCH).

followed and almost full hydrate conversion was achieved immediately after the unreacted ice was melted. A slight delay was observed from one MCH system as seen in the figure. However it was not observed in any other experiments. On the other hand, the hydrate growth for the TBME system was reasonably fast at 253 K but the effect of temperature ramping was not so drastic as in the case of the NH and MCH systems. This is probably due to the strong affinity between polar guest molecules like TBME with ice particles as indicated by the solubility and wetting properties of TBME with water/ice.[14,17] The strong interaction of TBME with water molecules makes it more difficult (higher energy barrier) for water molecules to reorientate and form hydrate cages resulting in slower kinetics.

Methane uptake with 50% LMGS synthesized at low pressure (P_0 = ~4.3 MPa)

Figure 4 shows the pressure drop profiles when the LMGS amount is less than the stoichiometric (50%). As seen, similar pressure drop profiles are observed as those with excess LMGS amounts. Rapid hydrate growth in stage I is seen to be followed by slower growth at stage II. However the rates for growth stage II, as indicated by the pressure drop, are higher for the NH and MCH systems. This is likely caused by the formation of sI hydrate. Some ice particles may be exposed directly to methane gas because of the insufficient amount of LMGS. TBME still exhibited the fastest kinetics (during stage I and II) followed by the NH and MCH systems. Upon melting the unreacted ice, the pressure dropped quickly indicating fast hydrate formation but then it rose back up and stayed at the equilibrium pressure of sI methane hydrate at 274 K (~2.9 MPa). This suggests that most of the hydrates formed were a mixture of sI and sH hydrates. However methane in sI hydrates was not stable at pressures below ~2.9 MPa. Consequently it decomposed as indicated by an increase in pressure. The solid state analysis showed that the solid phase contained mostly sH hydrate with a significant amount of unreacted ice and a small amount of sI hydrate. The hydrate yield was determined by dissociating the samples. It was found to be only ~15–25% for the NH and TBME systems although there was sufficient LMGS to convert up to ~50% theoretically. The yield for the MCH system was ~45% but it consisted of mixed sI and sH hydrates. The sH hydrate content was ~20%. This emphasizes the need to have excess LMGS to fully convert ice/water into hydrate. This is especially important in a nonstirred system.

Methane uptake with 200% LMGS synthesized at high pressure (P_0 = ~8.1 MPa)

At higher pressures, sI methane hydrate is also stable and hence a competition between sI and sH methane hydrate may well exist. However the solid-state analysis shows that sH hydrate is the observed structure when the LMGS is in excess. The methane uptake rate is shown in Figure 5. The initial reaction rates (stage I) were faster than those at lower pressure. But they were not significantly better as the growth was limited by the existence of a hydrate film. Further hydrate conversion at growth stage III was also observed upon melting the unreacted ice. However the rates were much slower than those synthesized at lower pressures. It took a week to achieve ~90% conversion at higher pressure whereas only several hours at lower pressure. The solid-state NMR revealed that the methane occupancy was higher when the hydrate was synthesized at higher pressure. It is unclear whether the slower methane uptake rate is the result of higher occupancy or because of the competition between sI and sH hydrate formation. sI hydrate may form quickly at first, then convert to sH hydrate at slower rate.

Methane uptake with 50% LMGS amount synthesized at high pressure (P_0 = ~8.1 MPa)

Figure 6 shows the methane uptake profile. The growth rates in stage I were similar to those observed in the previous systems. The MCH curve crossed over the NH curve after

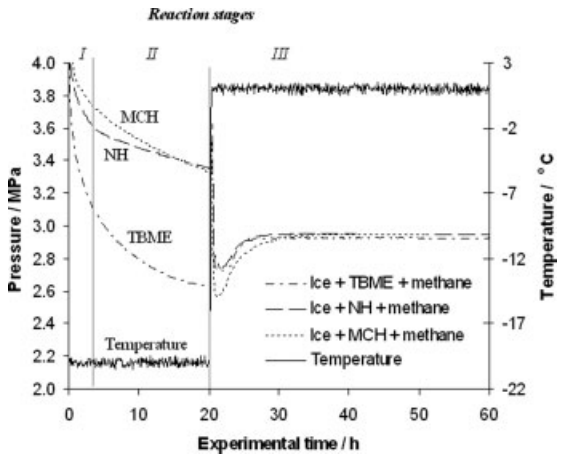

Figure 4. Pressure drop profile during hydrate formation from ice + LMGS (~50%) + methane synthesized at low pressure region (P_0 = ~4.3 MPa).

The LMGS used are *tert*-butyl methyl ether (TBME), neohexane (NH), and methylcyclohexane (MCH).

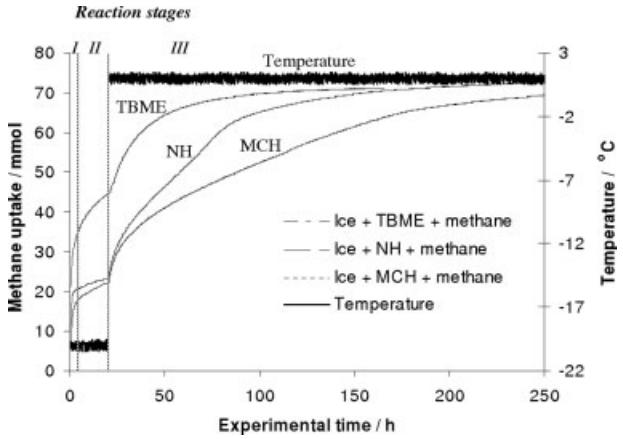

Figure 5. Amount of methane uptake during hydrate formation from ice + LMGS (~200%) + methane synthesized at high pressure (P_0 = ~8.1 MPa).

The LMGS used are *tert*-butyl methyl ether (TBME), neohexane (NH), and methylcyclohexane (MCH).

~1 h reaction time. This is most likely due to the formation of sI and sH hydrates mixture which increases the overall methane uptake. Higher slopes were also observed in growth stage II for all systems. After melting the unreacted ice core, slow and irregular methane uptake profiles were seen especially for NH and MCH systems. Higher overall methane uptake was also obtained confirming the presence of sI hydrate.

Methane uptake with no LMGS synthesized at high pressure (P_0 = ~8.1 MPa)

Hydrate formation kinetic of sI hydrate for the system with no LMGS and *n*-heptane as a nonhydrate former is shown in Figure 7. A noticeable lower methane uptake was observed in comparison to those from sH hydrates systems especially the reaction rate in stage I. The slope in growth stage II for ice-methane system is relatively higher than sH hydrate systems except with TBME. Rapid hydrate growth is also observed in stage III. The addition of *n*-heptane as a nonhydrate former appears to lower the uptake rates although the total methane uptake is comparable to that without one after a longer reaction time. The overall methane uptake for sI hydrate is higher than for sH hydrate due to higher methane storage capacity.

Methane uptake with the LMGS mixtures synthesized at low pressure (P_0 = ~4.3 MPa)

It is clear that the hydrate formation rate for the systems containing LMGS depends on the temperature where hydrate formation takes place. At temperatures below the icepoint where water molecules are relatively immobile (solid ice), LMGS which has the highest interaction/affinity towards water shows faster kinetics than a hydrophobic guest. This is clearly seen from the uptake rates of the TBME system that is superior to other LMGS systems in both stage I and II. However the strong affinity turns out to be a disadvantage when the water molecule is free to move around. Water soluble guest molecules inhibit the hydrate growth although hydrate seeds are present. Therefore only hydrophobic LMGSs like NH or MCH show rapid hydrate growth when the hydrate seeds are available and water molecules are mobile. The strong interaction between the water and LMGS also affects the methane occupancy and hence the gas stored in hydrate, as shown in Tables 2 and 3. This finding requires further attention and considerations in choosing the proper LMGS for gas storage and transport application. The kinetics observed during the hydrate formation and the gas content in the hydrate phase does not correlate as expected. Faster kinetics does

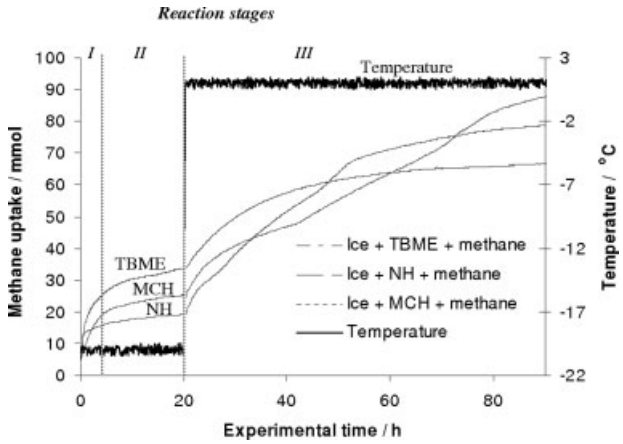

Figure 6. Amount of methane uptake during hydrate formation from ice + LMGS (~50%) + methane synthesized at high pressure (P_0 = ~8.1 MPa).

The LMGS used are *tert*-butyl methyl ether (TBME), neohexane (NH), and methylcyclohexane (MCH).

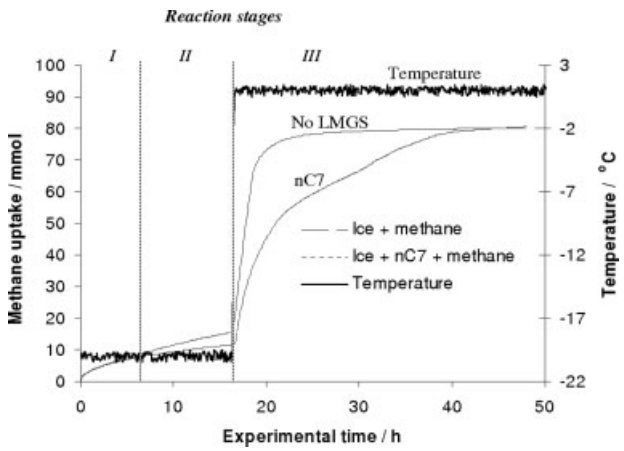

Figure 7. Amount of methane uptake during hydrate formation from ice without any LMGS synthesized at high pressure (P_0 = ~8.1 MPa).

The presence of *n*-heptane (*n*C7) as a nonhydrate former slows down the uptake rates however does not reduce the overall uptake.

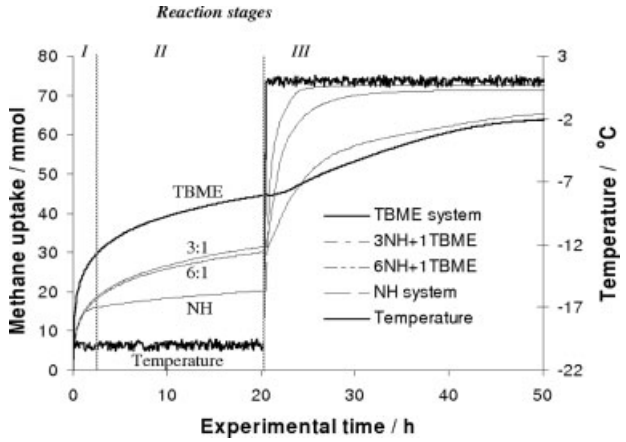

Figure 8. Amount of methane uptake during hydrate formation from ice + Neohexane (NH) and *tert*-butyl methyl ether (TBME) mixture (~200%) + methane, synthesized at low pressure (P_0 = ~4.3 MPa).

The addition of TBME together with a hydrophobic guest like NH enhances the methane uptake at temperature below the icepoint (253 K) however inhibits the formation rate at temperatures above the icepoint (274 K).

not necessarily give higher methane occupancy. Moreover, water soluble LMGS does not always offer the fastest kinetics especially in a nonstirred system. Hydrophobic LMGS have slower kinetics at the beginning but eventually reaches full conversion very rapidly with the temperature ramping and higher methane occupancy is obtained.

A mixture of TBME with NH at different concentrations was also studied in order to seek the optimum condition in terms of kinetics and methane occupancy. The idea was to see if the slow kinetics at the low temperature region (253 K) of NH system could be enhanced by the addition of small amount of TBME while maintaining the fast conversion rates at 274 K and high gas storage capacity in hydrate. The methane uptake curve that was obtained is shown in Figure 8. As seen, the addition of TBME did improve the conversion at 253 K. It is also seen that higher TBME concentration shifted the uptake curve closer to TBME profile. Methane occupancy/content was also reduced at higher TBME concentration, as seen in Tables 2 and 3. A similar result was also obtained with TBME and MCH mixtures. Hence adding TBME into other hydrophobic guest does not necessarily improve the overall conversion rate and maintain high methane content in hydrate phase. Only a small amount of TBME in the mixture (less than 20%) may improve the rate.

The total reaction time could be minimized with the knowledge of the hydrate growth stages. Approximately 2–3 h reaction time at a temperature below the icepoint is enough for stage I. The unnecessary time spent in growth stage II can be eliminated. Rapid hydrate growth towards full conversion is achievable with thermal ramping (stage III) for another ~5 h. Hence the total reaction time to fully convert ice into sH hydrates with maximum methane occupancy can be reached within ~8 h.

Correlation of conversion rate with crystallization models

Methane uptake curves at 253 K are fitted to crystallization kinetics models, using the well-known Avrami equations[18–20] for the initial reaction stage I and shrinking core model (SCM)[15,21] for stage II (diffusion through hydrate film). The equations are given below:

$$\text{Avrami: } \alpha = 1 - \exp(-k_1 t^n) \tag{1}$$

$$\text{SCM: } (1-\alpha)^{1/3} = \frac{-(2k_2)^{1/2}}{r}(t-t^*)^{1/2} + (1-\alpha^*)^{1/3} \tag{2}$$

where α is the hydrate conversion ratio at time t, α^* is the hydrate conversion ratio when diffusion though hydrate film starts at time t^*, k is the rate constant with the subscript indicating the growth stage, n is the Avrami exponent and r is the radius of ice particle (~0.65 μm[22]).

The hydrate conversion ratio as a function of time is regressed with both equations to obtain the rate constant k_1, k_2, and Avrami exponent n. The conversion values are calculated from the methane uptake profile divided by the total moles of methane that would be consumed if the ice particles are converted into hydrate completely taking into account the cage occupancy measured from NMR. It is important to note here that the Avrami equation is only valid at low crystal yield, up to a certain hydrate conversion ratio α^* before the hydrate film diffusion takes over where the SCM is more suitable to represent the data. The Avrami exponent n may explain the hydrate nucleation and growth mechanism.[23,24] The n-value increases with dimensionality of the growth, starting from unity for a free linear growth up to 3 for a three-dimensional growth. Instantaneous nucleation does not contribute any additional value to n however sporadic nucleation does. The maximum n-value is 4 when the crystal growth is in three-dimensions and sporadic nucleation is expected.[25] Mass transfer resistance such as diffusion controlled growth reduces the value of n, typically by half.[23]

Correlation with the Avrami model

The typical Avrami plots are shown in Figures 9 and 10 for the hydrate systems with excess LMGS amount synthesized at low and high pressure condition. The slopes from the plot correspond to the Avrami exponent n. The correlations from the Avrami model to the measured conversion rate are shown in Figures 11 and 12. As seen, the Avrami model fits quite well the hydrate conversion ratio data during stage I. The calculated conversion using the Avrami equation over-estimates the data after a certain hydrate conversion ratio (α^*) has been reached (t^*). The slope in this region corresponds to hydrate growth that is limited by the diffusion through hydrate film. Hydrate conversion in this region will be discussed in the later section with the SCM.

Linear correlations are seen in different regions at 253 K. The first region is observed on the MCH and/or NH systems only. The other two regions are present in all systems. A sharp slope ($n > 0.75$) at the beginning in Figure 9 may be ascribed to the slow diffusion of methane in MCH. The model slightly over-estimates the data in this region, as seen for the MCH system in the first 30 min in Figure 11. This is

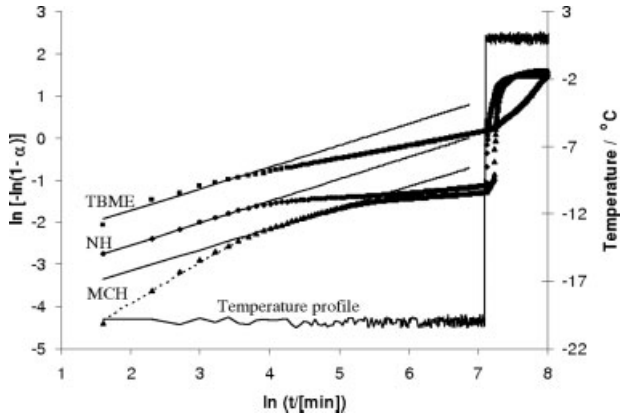

Figure 9. Avrami plot for ice + LMGS (~200%) + methane hydrate systems synthesized at low pressure (P_0 = ~4.3 MPa).

Initial steep slope (dashed line) is observed for MCH (methylcyclohexane) system, which may be ascribed to methane diffusion in MCH. The solid lines correspond to surface reaction at ice-LMGS liquid interface, fitted with Avrami equation with the regressed parameters given in Table 4. Hydrate formation in this region is controlled by methane diffusion in LMGS with the Avrami exponent $n \sim 0.5$. The slope become lower as hydrate film forms and covers the ice surface.

not seen in the NH or TBME system where methane diffusion is faster. NMR studies also confirmed the slow methane diffusion in MCH.[14] The slope changes to ~0.5 after the LMGS is saturated with methane. Solid lines in Figure 9 show that the slopes for all LMGS systems are parallel to each other with the *n*-value at around ~0.5. For a system where there is no resistance (free growth) with linear growth in one-dimension and instantaneous nucleation, the expected value of *n* is one. The observed *n*-value in this study is half

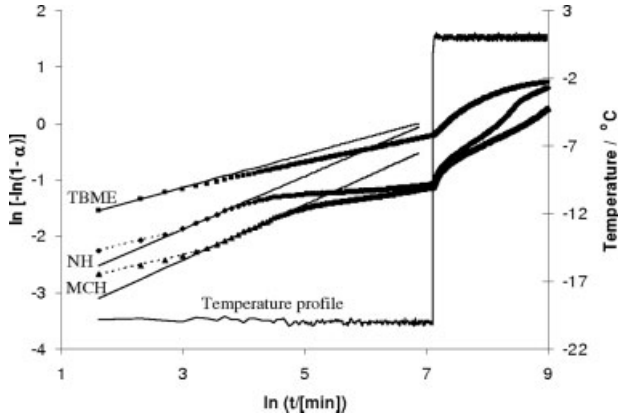

Figure 10. Avrami plot for ice + LMGS (~200%) + methane hydrate systems synthesized at high pressure (P_0 = ~8.1 MPa).

Initial moderate slopes (dashed line) are observed for neohexane (NH) and methylcyclohexane (MCH) systems, which may be ascribed to the formation of sI hydrate. The solid lines correspond to surface reaction at ice-LMGS liquid interface, fitted with Avrami equation with the regressed parameters given in Table 4. Hydrate formation in this region is controlled by methane diffusion in LMGS with the Avrami exponent $n \sim 0.5$. TBME (*tert*-butyl methyl ether) has lower slopes due to very fast reaction at high pressure so that hydrate film diffusion limits the reaction.

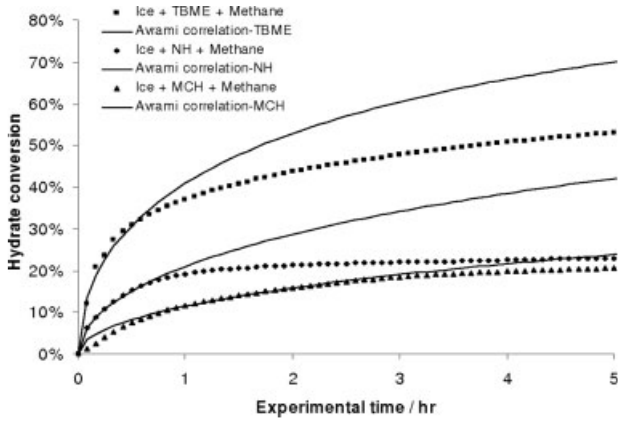

Figure 11. Hydrate conversion for ice + LMGS (~200%) + methane system synthesized at low pressure (P_0 = ~4.3 MPa).

The Avrami model correlates well with the experimental data up to ~20% conversion for neohexane (NH) and methylcyclohexane (MCH) systems and ~33% for *tert*-butyl methyl ether (TBME) system. The Avrami exponent *n* is 0.5.

from the expected *n*-value, which indicates that the crystal growth is controlled by methane diffusion in the LMGS liquid.

Morphology and gas uptake study are employed to justify that hydrate crystals grow in one dimension (rod-like growth[25]) with instantaneous nucleation. Lee et al.[26] showed that hydrate nucleation is spontaneous on a single or multiple sites until a hydrate film covered the surface in a short time period. The nuclei always appear all at once at the beginning. Sporadic nucleation where the nuclei appear at different times was never reported. Hairy-like or needle-like crystal morphologies were observed from water droplet and plane water/gas interface studies at the beginning of hydrate formation.[26–28] The primary arm grew inward to the liquid phase

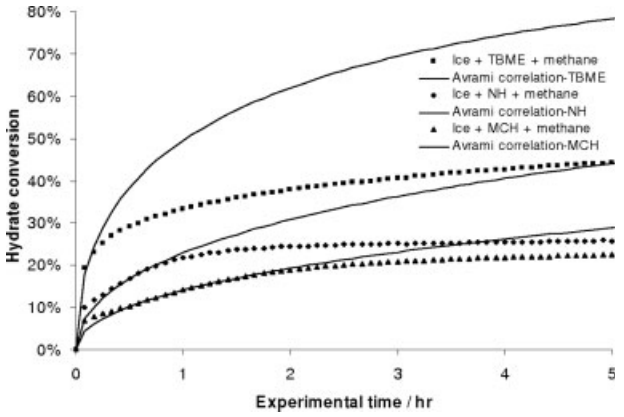

Figure 12. Hydrate conversion for ice + LMGS (200%) + methane system synthesized at high pressure (P_0 = ~8.1 MPa).

The Avrami model correlates well with the experimental data up to ~20% conversion for neohexane (NH) and methylcyclohexane (MCH) systems and ~25% for TBME system. The Avrami exponent *n* is 0.5.

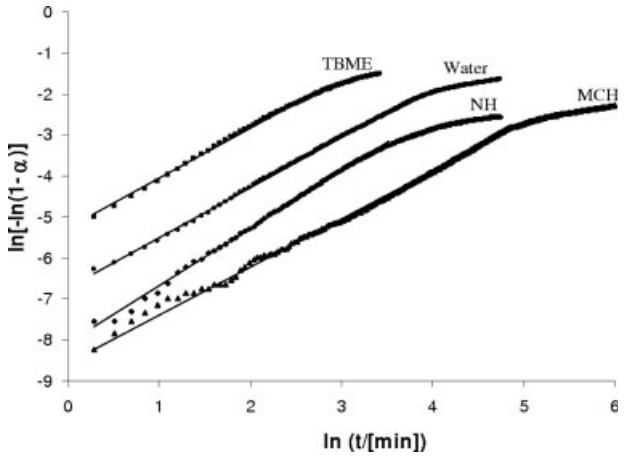

Figure 13. Avrami plot for water + LMGS (~200%) + methane systems.

Hydrates were synthesized at 275.35 K and 1 MPa above the corresponding hydrate equilibrium pressure. The solid lines correspond to the correlation with the Avrami equation at the initial hydrate growth. The Avrami exponent n is ~1.2 for most systems except for NH ($n \approx 1.4$). The intercepts correspond to the rate constant. Formation with TBME was the fastest followed by the water (no LMGS), NH, and MCH systems. Slower conversion rates are observed after a certain hydrate conversion is achieved, as seen by the reduced in slope.

from interface studies and outward to the gas phase from the droplet study initially. The secondary arm grew at a later time, generally at higher sub-cooling and a smoother crystal surface was typically observed after a longer period.

Figure 13 shows the Avrami plots from the gas uptake data we published earlier.[13] Hydrate was grown from a liquid water phase with mixing, so the resistances are assumed to be negligible. Instantaneous nucleation was also observed. The slopes are parallel for each system with the Avrami exponent n at around ~1.2 (except NH system at ~1.4). The n-value is slightly higher than one, most probably due to the contribution from the secondary arm growth (not completely linear). Hydrate crystal growth may actually consist of two stages. The first stage occurs rapidly and dominates the crystal growth front initially. It is the primary crystallization process where the radial growth from the center of the nuclei is observed, forming a needle-like crystal. The secondary growth stage is the slow crystallization process that may be indicated by thickening the crystal edges or crystal perfection forming a plate-like crystal. Since the secondary arm was reported to appear at a later time, perhaps it is safe to assume linear crystal growth ($n \approx 1$), which is true at the beginning of the reaction. The methane diffusion in LMGS lowers the Avrami exponent by a factor of two compared to the systems without mass transfer resistances.

The Avrami plots at higher pressure have a slightly different trend, as shown in Figure 10. The sharp slope in the first region is not seen anymore but a more gradual one is observed ($n < 0.5$). The NH system also shows a similar but smaller slope. This may suggest the formation of sI hydrate that is preferable/faster instead of sH hydrate with NH or MCH. However this does not last long, typically less than 30 min as seen in Figure 12 for NH and MCH systems. Perhaps some ice powders are exposed to methane gas initially to form sI hydrate. The slopes in the following two regions have similar trends as compared to those at low pressures ($n = \sim 0.5$) except for the TBME system. A gentler slope ($n < 0.5$) for the TBME system is due to rapid hydrate conversion at high pressure. A hydrate film forms quickly and this lowers the observed slope. It is also noted that the system with TBME does not have the first region because the methane diffusivity and the reaction rate of sH hydrate is faster than sI hydrate.

The Avrami plot for non-LMGS systems (sI hydrate) is also shown in Figure 14 for comparison. It is noted that for the ice-methane system, no gas diffusion in liquid phase exists. The initial hydrate formation or surface "reaction" (stage I) should occur really fast because there is no expected resistance for the ice surface to be in contact with the methane gas. Thus the expected n-value is one. Surprisingly the n-value obtained is even less than those with LMGS ($n = 0.4$). This suggests the presence of gas film which creates a concentration gradient around the ice particles. Hence methane has to diffuse through this film in order to react with ice and form hydrate. This gas film was also observed from the NMR study.[14] It is unknown whether the gas film is also present with LMGS. The expected slope would be lower than those without LMGS if the gas film is also present because of the additional resistance. However this was not seen and hence the existence of gas film is unlikely or insignificant. Consequently the observed rates with the presence of liquid LMGS are not necessarily lower than those without one although additional liquid layer is present. A lower n-value for sI hydrate in the initial reaction agrees with the lower slopes observed in the LMGS systems where the hydrate is synthesized at high pressure and less than stoichiometric LMGS amounts. The presence of n-heptane liquid is expected to behave in the same way as LMGS. Hence the expected n-value is ~0.5, which is indeed the value obtained. The slope for hydrate formation during stage II (hydrate film

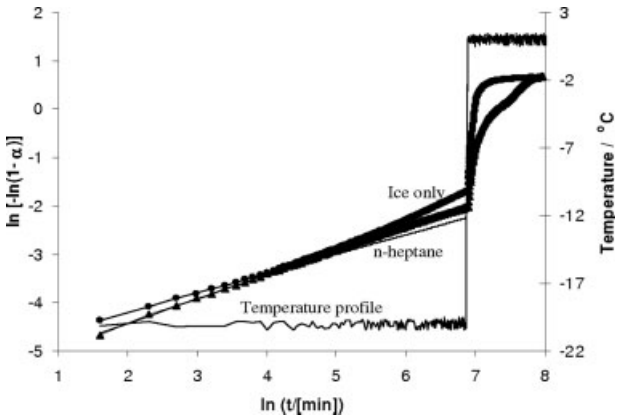

Figure 14. Avrami plot for ice + methane systems (no LMGS).

Hydrates were synthesized at high pressure ($P_0 = \sim 8.1$ MPa). The solid lines correspond to the reaction of methane with ice at the surface, fitted with Avrami equation. The Avrami exponent n is ~0.4 for ice and 0.5 for n-heptane. The expected lower slope in hydrate film diffusion controlled region (stage II) for n-heptane system is not clearly seen because of low conversion.

Table 4. Avrami Parameters, k is Given in Conversion/Minute^n

LMGS System/Amount	Pressure	k_1*	$n^{\dagger}$	k_1 (n = 0.5)
Ice + methane	High	0.0067	0.40	0.0048
Ice + methane + nC7	High	0.0043	0.51	0.0044
50% TBME	Low	0.0649	0.46	0.0601
	High	0.0331	0.54	0.0374
200% TBME	Low	0.0640	0.52	0.0671
	High	0.1358	0.28	0.0757
50% NH	Low	0.0272	0.52	0.0281
	High	0.0299	0.51	0.0305
200% NH	Low	0.0278	0.52	0.0302
	High	0.0378	0.47	0.0336
50% MCH	Low	0.0158	0.50	0.0155
	High	0.0167	0.51	0.0172
200% MCH	Low	0.0157	0.50	0.0158
	High	0.0205	0.49	0.0196

*The maximum standard error of k_1 is 5%
†The maximum standard error of n is 0.1.

Table 5. Shrinking Core Model Parameters

LMGS System/ Amount	Pressure	α* [conversion]	t*, h	$k_2^{\dagger}$, nm^2/h
Ice only	High	0.10	7	42
200% nC7	High	0.08	7	11
50% TBME	Low	0.22	0.5	400
	High	0.27	0.5	194
200% TBME	Low	0.33	0.5	399
	High	0.25	0.5	189
50% NH	Low	0.23	1	41
	High	0.17	1	7
200% NH	Low	0.20	1	12
	High	0.23	1	6
50% MCH	Low	0.17	3	51
	High	0.21	3	10
200% MCH	Low	0.20	3	3
	High	0.21	3	7

†The maximum standard error of k_2 is 3%.

diffusion controlled) for the methane-ice system is higher than in stage I with the slope at ~0.66. Apparently at this stage the gas film has disappeared so that a higher slope results. However it is still below one, which indicates resistance because of hydrate film.

The differences in observed intercepts from all Avrami plots correspond to different rate constants k_1. The higher the k_1 values are, the faster the hydrate conversion. TBME systems always appear at the top because they have the fastest kinetics followed by NH and MCH systems. The regressed k_1 and n-values are given in Table 4. The values correspond to the best fit from the data. However for comparison purposes, the k_1 values at n = 0.5 are also given so that the unit of k_1 is conversion/min$^{1/2}$. This allows the k_1 to be evaluated with respect to experimental variables, namely the pressure and LMGS type/amount without affecting the fit much. As seen in Table 4, it is clear that TBME has the fastest conversion rate among all LMGS investigated. The k_1 values

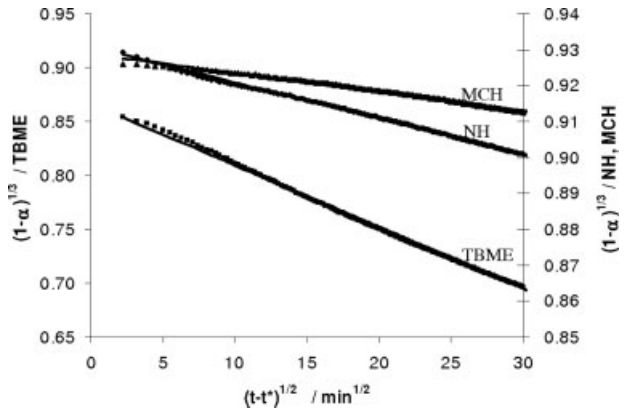

Figure 15. Shrinking core model (SCM) plot for ice + LMGS (~200%) + methane systems.

Hydrate was synthesized at low pressure (P_0 = ~4.3 MPa). The SCM plots are linear and in good agreement with the experimental data. A slight deviation is seen at the beginning, most probably due to the incomplete transition from stage I (surface reaction) to stage II (hydrate film diffusion).

increase with pressure, except for the case with 50% TBME because of the formation of sI hydrate. A lower LMGS amount reduces the k_1 values slightly. The rate constant k_1 for sI hydrate is actually lower than that for sH hydrate. Hence the presence of LMGS liquid layer on the ice surface does not necessarily limit the hydrate conversion because of high solubility of methane in LMGS liquid phase.

Correlation with the shrinking core model

As mentioned in the previous section, the third and last slope (stage III) corresponds to hydrate film diffusion controlled formation. The presence of the hydrate layer on the ice surfaces limits the mass transfer so that the subsequent hydrate growth becomes much slower. A SCM is employed in this region to fit the data. A typical SCM plot is shown in Figure 15. As seen, the model fits the data well. A slight deviation is observed for the first few data points, as also indicated by Wang et al.[15] Perhaps this is due to the transition from surface "reaction" to hydrate film diffusion controlled "reaction." The value of α*, t*, and the rate constant k_2 is given in Table 5. Generally the conversion rate starts to decrease after ~20% of ice has been converted into hydrate. The time required to achieve this depends on the crystal growth rate for the previous region, which varies between 30 min and 3 h. The growth rate constant k_2 at this point varies between ~3 and 400 nm^2/h. NH and MCH system have the lowest k_2, between 3 and 10 nm^2/h. Hence the subsequent growth after the first ~3 h is almost negligible. The TBME system has the highest α* (~30%) and k_2 values (~400 nm^2/h) implying a strong interaction between ice and TBME. For the system with 50% LMGS, the k_2 values are affected by the formation of sI hydrate. The k_2 value for the methane-ice system is higher than for NH and MCH systems but lower than for TBME. Thus the k_2 values increase for NH and MCH system but decrease for the TBME system when sI hydrate coexists with sH hydrate in this region.

Conclusions

sH hydrates were synthesized from fresh-ground ice powder. Three sH hydrate formers were selected in this study:

tert-butyl methyl ether (TBME), neohexane (NH), and methylcyclohexane (MCH). The number of moles of methane consumed and hydrate conversion were determined and compared with crystallization kinetics models. The hydrate crystallization "reaction" was allowed to proceed for 20 h at 253 K before ramping the temperature to 274 K. This hydrate synthesis procedure was found to be the best in obtaining full hydrate conversion (more than 90% conversion) within a short time and without mixing. Hydrates were found to grow in three "reaction" stages. The first stage lasted about 30 min to 3 h until a certain degree of hydrate conversion was achieved ($\sim$20% for NH and MCH, $\sim$30% for TBME, $\sim$10% for sI hydrate). The conversion rates in this region (stage I) were well correlated by the Avrami equation. The Avrami exponent (n) was found to be $\sim$0.5, which suggests that hydrate nucleated instantaneously and grew in one-dimension (rod-like) with methane diffusion into the LMGS liquid controlling the "reaction". The subsequent "reaction" (stage II) was much slower because of the formation of a hydrate film on the ice surface that impeded the mass transfer. A SCM was able to fit the data well. The TBME system appeared to have the fastest kinetics followed by NH and MCH systems in both "reaction" stages. However the trend changed when the temperature was increased ("reaction" stage III). Most likely this is attributed to the strong interaction between TBME and liquid water molecules.

The conversion rates were found to depend on the amount of LMGS, the temperature and pressure at which the hydrate was synthesized. An excess amount of LMGS was required to maintain sH hydrate formation. The conversion rates were faster when the pressure was below the stability region of sI hydrate at temperatures above the icepoint. Higher pressures slowed down the kinetics although higher methane content in the hydrate phase was also noted. Adding TBME into NH or MCH may help enhance the conversion rate at 253 K but not at 274 K. The amount of methane stored in hydrate was also reduced in the system with TBME depending on the concentration used. Finally, NH was found to the best LMGS in this study to obtain full conversion within a short reaction time and achieving high methane gas storage in the hydrate.

Acknowledgments

The financial support from Natural Sciences and Engineering Research Council of Canada (NSERC) is greatly appreciated. Robin Susilo gratefully acknowledges financial support from Canada Graduate Scholarship (CGS).

Literature Cited

1. Tsuji H, Kobayashi T, Ohmura R, Mori YH. Forming structure-H hydrates using water spraying in methane gas: effects of chemical species of large-molecule guest substances. *Energy Fuels*. 2005; 19:869–876.
2. Sun Z, Wang R, Ma R, Guo K, Fan S. Effect of surfactants and liquid hydrocarbons on gas hydrate formation rate and storage capacity. *Energy Convers Manage*. 2003;44:2733–2742.
3. Gudmundsson JS, Andersson V, Levik OI, Mork M. Hydrate technology for capturing stranded gas. *Ann NY Acad Sci*. 2000;912:403–410.
4. Abdalla BK, Abdullatef NA. Simulation and economic evaluation of natural gas hydrates [NGH] as an alternative to LNG. *Catal Today*. 2005;106:256–258.
5. Javanmardi J, Nasrifar KH, Najibi SH, Moshfeghian M. Economic evaluation of natural gas hydrate as an alternative for natural gas transportation. *Appl Therm Eng*. 2005;25:1708–1723.
6. Thomas S, Dawe RA. Review of ways to transport natural gas energy from countries which do not need the gas for domestic use. *Energy*. 2003;28:1461–1477.
7. Sloan ED. *Clathrate Hydrates of Natural Gases*, 2nd edition. New York: Marcel Decker, 1998.
8. Schicks JM, Ripmeester JA. The coexistence of two different methane hydrate phases under moderate pressure and temperature conditions: kinetic versus thermodynamic products. *Angew Chem Int Ed*. 2004;43:3310–3313.
9. Chou IM, Sharma A, Burruss RC, Shu J, Mao HK, Hemley RJ, Goncharov AF, Stern LA, Kirby SH. Transformation in methane hydrate. *PNAS*. 2000;97:13484–13487.
10. Loveday JS, Nelmes RJ, Klug DD, Tse JS, Desgreniers S. Structural systematics in the clathrate hydrates under pressure. *Can J Phys*. 2003;81:539–544.
11. Kumazaki T, Kito Y, Sasaki S, Kume T, Shimizu H. Single-crystal growth of the high-pressure phase II of methane hydrate and its Raman scattering study. *Chem Phys Lett*. 2004;388:18–22.
12. Khokhar AA, Gudmundsson JS, Sloan ED. Gas storage in structure H hydrates. *Fluid Phase Equilib*. 1998;150:383–392.
13. Lee JD, Susilo R, Englezos P. Kinetics of structure H gas hydrate. *Energy Fuels*. 2005;19:1008–1015.
14. Susilo R, Moudrakovski IL, Ripmeester JA, Englezos P. Hydrate kinetics study in the presence of non-aqueous liquid by NMR spectroscopy and imaging. *J Phys Chem B*. 2006;110:25803–25809.
15. Wang X, Schultz AJ, Halpern Y. Kinetics of methane hydrate formation from polycrystalline deuterated ice. *J Phys Chem A*. 2002; 106:7304–7309.
16. Susilo R, Ripmeester JA, Englezos P. Characterization of gas hydrates with PXRD, DSC, NMR and Raman spectroscopy. *Chem Eng Sci*. 2007;62:3930–3939.
17. Susilo R, Lee JD, Englezos P. Liquid–liquid equilibrium data of water with neohexane, methylcyclohexane, tert-butyl methyl ether, n-heptane and vapor–liquid–liquid equilibrium with methane. *Fluid Phase Equilib*. 2005;231:20–26.
18. Avrami M. Kinetics of phase change. I. General theory. *J Chem Phys*. 1939;7:1103–1112.
19. Avrami M. Kinetics of phase change. III. Granulation, phase change, and microstructure. *J Chem Phys*. 1941;9:177–184.
20. Avrami M. Kinetics of phase change. III. Granulation, phase change, and microstructure kinetics of phase change. *J Chem Phys*. 1941;9:177–184.
21. Fujii K, Kondo W. Kinetics of the hydration of tricalcium silicate. *J Am Ceram Soc*. 1974;57:492–497.
22. Moudrakovski IL, Sanchez AA, Ratcliffe CI, Ripmeester JA. Nucleation and growth of hydrates on ice surfaces: new insights from 129Xe NMR experiments with hyperpolarized Xenon. *J Phys Chem B*. 2001;105:12338–12347.
23. Gedde UW. *Polymer Physics: Crystallization Kinetics*. London: Chapman and Hall, 1995:169–199.
24. Marangoni AG. *Fat Crystals Network: Crystallization Kinetics*. New York: Marcel Dekker, 2005:21–83.
25. Shaples A. *Introduction to Polymer Crystallization*. London: Edward Arnold, 1966:44–59.
26. Lee JD, Susilo R, Englezos P. Methane–ethane and methane–propane hydrate formation and decomposition on water droplets. *Chem Eng Sci*. 2005;60:4203–4212.
27. Lee JD, Song M, Susilo R, Englezos P. Dynamics of methane-propane clathrate hydrate crystal growth from liquid water with or without the presence of *n*-Heptane. *Cryst Growth Des*. 2006;6:1428–1439.
28. Servio P, Englezos P. Morphology study of structure H hydrate formation from water droplets. *Cryst Growth Des*. 2003;3:61–66.

Manuscript received Apr. 25, 2007, and revision received Jun. 6, 2007.